Thin Solid Films 520 (2012) 6576–6580

Contents lists available at SciVerse ScienceDirect

Thin Solid Films

journal homepage: www.elsevier.com/locate/tsf

A map of competing buckling-driven failure modes of substrate-supported thin brittle films

Zheng Jia [a], Cheng Peng [b], Jun Lou [b,*], Teng Li [a,*]

[a] Department of Mechanical Engineering and Maryland NanoCenter, University of Maryland, College Park, MD 20742, USA
[b] Department of Mechanical Engineering and Materials Science, Rice University, Houston, TX 77005, USA

ARTICLE INFO

Article history:
Received 27 January 2012
Received in revised form 21 June 2012
Accepted 6 July 2012
Available online 14 July 2012

Keywords:
Thin films
Cracking
Delamination
Buckling

ABSTRACT

Our in situ experiments of polyimide-supported thin indium tin oxide (ITO) films reveal *buckling-driven film cracking* in some samples and *buckling-driven interfacial delamination* in other samples. Although studies of individual buckling-driven failure mode exist, it still remains unclear what governs the competition between these two different failure modes in a given film/substrate structure. Through theoretical analysis and numerical simulations, we delineate a map of competing buckling-driven failure modes of substrate-supported thin brittle films in the parameter space of interfacial adhesion and interfacial imperfection size. Such a map can offer insight on the mechanical durability of functional thin films. For example, interestingly, we show that strongly bonded thin brittle films are more prone to buckling-driven cracking, a more detrimental failure mode for thin brittle ITO transparent conductors widely used in displays and flexible electronics.

© 2012 Elsevier B.V. All rights reserved.

1. Introduction

Substrate-supported thin films have found widespread applications in microelectronics and flexible electronics technology [1–4]. For example, thin indium tin oxide (ITO) films deposited on a polymer substrate are often used as transparent conductors and interconnect in flexible devices. As flexible electronic devices frequently experience large deformation, the mechanical failure of such thin films (e.g., ITO) poses significant challenge to the device reliability [5–7]. A common failure mechanism of substrate-supported thin films is compression-induced buckling or wrinkling. The compression in the film may result from residual stress (e.g., due to film/substrate thermal mismatch or from film growth), or from the Poisson's effect when the film/substrate laminate is subject to uniaxial tension. Well bonded to a rather compliant substrate (e.g., an elastomer), a thin film under compression can wrinkle coherently with the underlying substrate [8–11]; on a relatively stiff substrate, however, a thin brittle film under compression may partially delaminate from the substrate and buckle to mitigate the compression. In turn, the film buckling drives further growth of delamination [2,12–17]. Buckling-driven delamination of thin films on substrates has been extensively studied [2,12–17]. Recent experiments on substrate-supported thin brittle films in the context of flexible electronics, however, reveal the *buckling-driven cracking* of the thin brittle films (e.g. Fig. 1a), a different buckling-driven failure mode that is less studied [18–20]. In practice, the buckling-driven cracking of ITO films is more detrimental than the buckling-driven delamination of ITO films, as ITO film cracking cuts off the electrical conductance while a delaminated ITO strip can still carry electric currents. Although existing studies offer critical understanding of each of these buckling-driven failure modes, one key question that remains unanswered is: what governs the competition between buckling-driven interfacial delamination and bucking-driven film cracking in a given substrate-supported thin brittle film? Answers to such a question are of technological importance, e.g., shedding light on how to avoid buckling-driven film cracking in order to minimize the electrical conductance loss of polymer-supported ITO conductors in flexible devices. To address these unsolved issues, this paper delineates a theoretical analysis and carries out numerical simulations to quantitatively determine key parameters that govern the competition among different buckling-driven failure modes in a substrate-supported thin brittle film. Emerging from the present study is a map of three competing buckling-driven failure modes of substrate-supported thin brittle films in the parameter space of interfacial adhesion and interfacial imperfection size. Such a map can offer design guidelines to optimize the mechanical durability of functional thin films.

The rest of the paper is organized as follows. Section 2 presents the experimental observation of buckling-driven interfacial delamination and buckling-driven film cracking in polyimide-supported ITO films. Section 3 delineates a theoretical model to decipher the dominant buckling-driven failure mode for a given film/substrate structure subject to film compression. In Section 4, we study the effect of substrate stiffness on the buckling-driven failure modes of substrate-supported thin brittle films, using finite element modeling. A concluding remark is given in Section 5.

* Corresponding authors.
E-mail addresses: jlou@rice.edu (J. Lou), lit@umd.edu (T. Li).

0040-6090/$ – see front matter © 2012 Elsevier B.V. All rights reserved.
doi:10.1016/j.tsf.2012.07.011

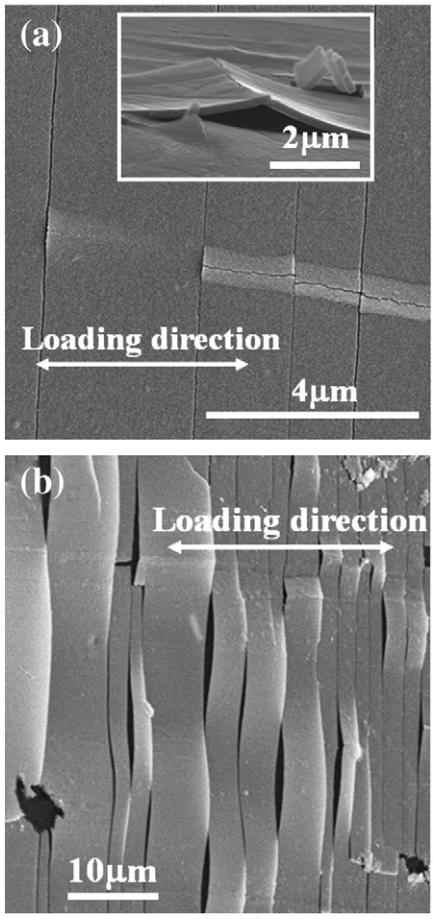

Fig. 1. (a) SEM image of a thin brittle ITO film (100 nm thick) on a thick polyimide substrate (75 μm thick) under uniaxial tension. The long strips along vertical directions result from tensile fracture of the ITO film and are then subject to Poisson's compression perpendicular to tension direction. Some ITO strips buckle away from the substrate and eventually crack at the crest along the direction roughly parallel to the applied tension. (Inset shows perspective view of buckling-driven film cracking in a different sample.) (b) In another polyimide-supported ITO film (80 nm thick), Poisson's compression in the ITO strips only leads to film delamination, without film cracking. Note that the widths of interfacial delamination in (b) are much longer than those in (a).

2. In situ experimental observation of buckling-driven failure of substrate-supported thin brittle films

ITO thin films were deposited on polyimide substrates (DuPont Kapton 50NH, 75 μm in thickness, well-cut in dog-bone shape with gauge length of 7 mm and width of 3 mm) by e-beam evaporation. Mixed ITO powder (In_2O_3 and SnO_2, weight ratio of 90%:10%, density of 7.14 g/cm^3) was used as the evaporation sources in a Sharon E-beam evaporator. The deposition rate was kept at ~1 Å/s and chamber pressure was at $\sim 1.33\times10^{-3}$ Pa. Before being loaded into the chamber, polyimide substrates were cleaned in an ultrasonic cleaner for 10 min with acetone and ethanol and then dried with nitrogen gas. The in situ tests were performed using a micro-tester (Deben UK Ltd.) inside the scanning electron microscope (SEM) chamber (FEI Quanta 400 high resolution field emission scanning electron microscope, FEI company, Hillsboro, Oregon).

Subject to uniaxial tension, channel cracks initiate and propagate in the polyimide-supported brittle ITO film along the direction perpendicular to the tension. More channel cracks appear as the applied tension increases and eventually the spacing between neighboring cracks saturates [7]. Upon further tension, some ITO strips (demarcated by two neighboring channel cracks) delaminate and buckle away from the substrate, driven by the compressive stress in the ITO film due to Poisson's effect. In some samples (e.g., Fig. 1a), the buckled portion of ITO film eventually cracks at the crest along the direction roughly parallel to the applied tension. By contrast, in other samples (e.g., Fig. 1b), the similar ITO strips are found to only delaminate and buckle under Poisson's compression, without film cracking. The length of the delaminated portion of the ITO film in the latter case is found to be much longer than that in the buckling-driven cracking case.

3. A map of buckling-driven failure modes of substrate-supported thin brittle films

To understand the experimental observation described in Section 2, in the present section we delineate a theoretical model to decipher the dominant buckling-driven failure mode for a given film/substrate structure subject to film compression. Fig. 2a illustrates the schematics of the model. A thin brittle film of thickness h on an infinitely thick elastic substrate of width B is subject to film compression ε_f. An initial imperfection is introduced as a delamination of width $2b$ at the center location of the interface. When ε_f exceeds the critical Euler buckling strain $\varepsilon_{cr} = -\pi^2h^2/(12b^2)$, the delaminated portion of the film buckles with an out-of-plane amplitude profile of

$$w(x) = (A/2)[1 + \cos(\pi x/b)], \tag{1}$$

where A is the peak amplitude of the buckled portion.

The out-of-plane film buckling provides driving force for further growth of delamination, which increases as the buckling amplitude increases. We next determine a critical buckling amplitude A_d^{cr}, above which the initial interfacial delamination starts to advance. The total potential energy of the system is given by

$$U_{total} = U_{unbuckled} + U^m_{buckled} + U^b_{buckled} - (B-2b)\Gamma, \tag{2}$$

where $U_{unbuckled}$ is the strain energy of the film portion still bonded to the substrate, $U^m_{buckled}$ and $U^b_{buckled}$ are the membrane energy and bending energy of the buckled portion of the film, respectively, and Γ is the film/substrate interfacial adhesion energy. Here in the theoretical model we assume that the substrate is rigid, thus the substrate strain energy is not included in U_{total} (the effect of substrate stiffness will be considered later

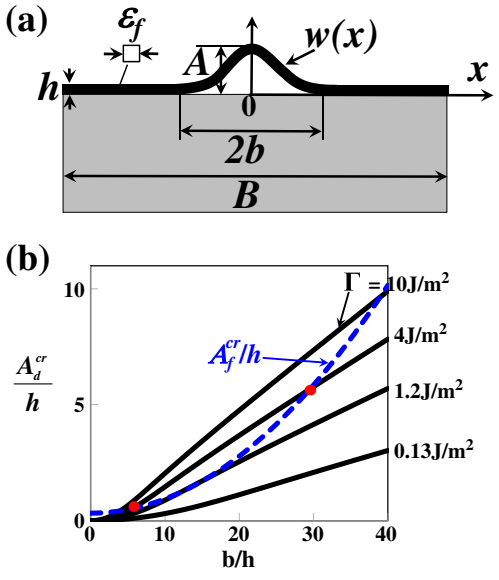

Fig. 2. (a). A schematic of the model (not to scale). (b). Solid lines plot A_d^{cr}/h as a function of b/h, for various values of interfacial adhesion Γ. Dashed line plots A_f^{cr}/h as a function of b/h.

in Section IV through numerical simulations). The unbuckled portion of the film is only subject to membrane compression ε_f, so

$$U_{unbuckled} = (B-2b)h\left(E'_f\varepsilon_f^2/2\right), \tag{3}$$

where E'_f is the plane strain Young's Modulus of the film. For the buckled portion of the film,

$$U^m_{buckled} = bhE'_f\varepsilon_x^2, \tag{4}$$

where $\varepsilon_x = \varepsilon_f + (\pi A/4b)^2$ (the latter term denotes the contribution of bending to the non-linear membrane strain in the buckled portion of the film), and

$$U^b_{buckled} = \int_{-b}^{b}\left(E'_f h^3/24\right)\left(\frac{d^2w}{dx^2}\right)^2 dx = E'_f\pi^4A^2h^3/96b^3. \tag{5}$$

Energy minimization of U_{total} with respect to A and b gives a critical buckling amplitude

$$\frac{A_d^{cr}}{h} = \sqrt{\frac{8}{3}\left(\sqrt{1+\frac{9\Gamma}{2E'_f h}\left(\frac{2b}{\pi h}\right)^4}-1\right)}, \tag{6}$$

above which the initial delamination starts to advance.

Fig. 2b plots A_d^{cr}/h as a function of b/h, for various values of interfacial adhesion energy Γ (solid lines). Here, $E'_f = 132$ GPa, which is representative for ITO. A_d^{cr} increases monotonically as Γ or b increases. That is, a stronger interfacial adhesion or a longer initial interfacial defect makes the film more resistant to further interfacial delamination.

We next determine the critical buckling amplitude above which fracture occurs at the crest of the buckled portion of the film. The total strain in the buckled portion of the film consists of the contribution from the compressive membrane strain ($=-\pi^2h^2/(12b^2)$), and that from the bending strain, which varies from tensile to compressive across the film thickness and is linearly proportional to film curvature $\frac{d^2w}{dx^2}$. Therefore, if the film buckles severely, the strain at the top surface of the buckled crest, given by $\frac{\pi^2h^2}{4b^2}\left(\frac{A}{h}-\frac{1}{3}\right)$, may become tensile and exceed the fracture strain of the brittle film material, causing film cracking at the crest. The above argument gives a critical buckling amplitude, above which buckling-driven cracking of the film occurs,

$$\frac{A_f^{cr}}{h} = \frac{1}{3}+\left(\frac{2b}{\pi h}\right)^2\frac{\sigma_f}{E'_f}, \tag{7}$$

where σ_f is the fracture strength of the brittle film material. The dashed line in Fig. 2b plots A_f^{cr}/h as a function of b/h, for the case of $\sigma_f = 2$ GPa and $E'_f = 132$ GPa (representative for ITO). A_f^{cr} increases monotonically as b increases.

Note that the buckled portions of the film near two delaminating fronts are also subject to bending. On a rigid substrate, severe buckling of a film may also cause film cracking initiating from the bottom surface of the film near the delaminating fronts [21]. However, such cracking events most likely occur after the film cracking at the crest, as the film bending near the delaminating fronts is partially constrained by the rigid substrate thus leads to a lower film stress level than that at the crest. On a compliant substrate, the film cracking near the delaminating fronts is less likely to occur as the substrate can be distorted near the fronts to accommodate the local deformation of the film and thus to mitigate the film stress. Above said, the present model only consider the competition between the film cracking at the crest and the film/substrate interfacial delamination, two dominant buckling-driven failure modes of substrate-supported thin brittle films.

The comparison of the two critical buckling amplitudes defined in Eqs. (6) and (7) determines the dominant buckling-driven failure mode of a given film/substrate structure (e.g., E'_f, σ_f, and Γ) with an interfacial delamination of width $2b$ under sufficient film compression. That is, if $A_d^{cr} < A_f^{cr}$, buckling-driven delamination occurs; while if $A_f^{cr} < A_d^{cr}$, buckling-driven film cracking occurs.

As shown in Fig. 2b, there exists a critical value of interfacial adhesion energy Γ (≈ 1.2 J/m^2), below which $A_d^{cr} < A_f^{cr}$ for all values of b/h. In other words, if the interface is weak (e.g., $\Gamma < 1.2$ J/m^2), large compression in the film always leads to the further advancement of the initial delamination, which mitigates the film compression in the buckled portion. Therefore, no buckling-driven film cracking occurs. For a given $\Gamma > 1.2$ J/m^2, the A_f^{cr} vs. b/h curve intersects the A_d^{cr} vs. b/h curve at two points. For example, the two curves intersect at $b/h = 5.6$ and 29.4 for $\Gamma = 4$ J/m^2. When $b/h < 5.6$, $A_d^{cr} < A_f^{cr}$. As a result, under sufficient film compression, the initial delamination starts to advance until $b/h = 5.6$, after which $A_d^{cr} \geq A_f^{cr}$. In other words, the failure mode is buckling-driven delamination first, followed by film cracking. When $5.6 < b/h < 29.4$, $A_f^{cr} < A_d^{cr}$. As a result, the buckled portion of the film always cracks at the crest before any further advancement of the initial delamination. When $b/h > 29.4$, $A_d^{cr} < A_f^{cr}$, which means that the initial delamination always advance under sufficient film compression but no film cracking can occur. The above comparison between the two critical buckling amplitudes defined in Eqs. (6) and (7) delineates three buckling-driven failure modes: A). Buckling-driven delamination followed by film cracking, B). Buckling-driven film cracking without delamination, and C). Buckling-driven delamination without film cracking.

Fig. 3 plots a map of these three failure modes in the parameter space of interfacial adhesion energy and initial interfacial defect size. When the interfacial adhesion energy is lower than a critical value (≈ 1.2 J/m^2 when $b/h < 26.5$, and slightly higher when $b/h > 26.5$), buckling-driven delamination dominates and film cracking does not occur (Mode C). When the interfacial adhesion energy is higher than the critical value, buckling-driven film cracking occurs, either after a modest propagation of interfacial delamination if the initial interfacial defect is small (Mode A) or without interfacial delamination if the initial interfacial defect is large (Mode B).

It is worthy to note that the main focus of the present study is to decipher the competition between buckling-driven interfacial delamination and buckling-driven film cracking, rather than each individual buckling-driven failure mode. Analytic models that are more sophisticated than those in the present study could be derived from existing studies on either buckling-driven interfacial delamination or buckling-driven film cracking and adopted to investigate the failure mode competition. It is expected that such more sophisticated treatments should lead to a map of buckling-driven failure modes similar to that delineated in Fig. 3, with differences being quantitative, rather than qualitative.

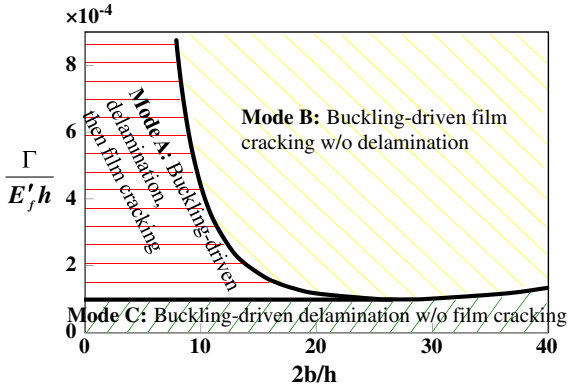

Fig. 3. A map delineates three buckling-driven failure modes in the parameter space of interfacial adhesion energy and initial interfacial defect size, namely, A) buckling-driven delamination followed by film cracking, B) Buckling-driven film cracking without delamination and C) Buckling-driven delamination without film cracking.

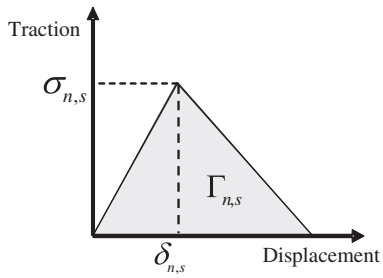

Fig. 4. The traction-displacement laws used to model the ITO/polymer interface.

4. Effect of substrate stiffness on the map of buckling-driven failure modes

In our analytic model, the substrate is assumed to be rigid. To investigate the effect of substrate stiffness on the buckling-driven failure modes of substrate-supported thin brittle films, we perform finite element modeling to simulate the full process of buckling-driven failure.

The film/substrate laminate is assumed to deform under plane strain condition (e.g., Fig. 2a). In the simulation model, the film is a layer with thickness of h and the substrate is a block with thickness of 50 h and width of $B=200$ h. Both the film and the substrate are modeled as linear elastic materials. The Young's Modulus and the Poisson's ratio of the film are 120 GPa and 0.3, respectively. The Young's Modulus of the substrate varies from 2 GPa to 20 GPa, with a Poisson's ratio of 0.4. The film is densely meshed with four-node plane strain elements with element size of 0.1 h. The substrate is also meshed with four-node plane strain elements with matching element size near the interface and coarse elements far away from the interface. The film compression is introduced as a thermal mismatch strain. An initial interfacial delamination of various widths is prescribed at the center location of the interface. The simulations are carried out using finite element code ABAQUS v6.9. To simulate the buckling-induced delamination, the bonded portion of the interface is modeled with cohesive elements, which are characterized by a tensile and a shear traction-displacement law, with six parameters: interfacial tensile strength σ_n and shear strength σ_s, critical opening displacement δ_n and sliding displacement δ_s, and the areas under the traction-displacement curve Γ_n and Γ_s (the normal and shear interfacial adhesion energy of the ITO/polymer interface, respectively), as illustrated in Fig. 4. We assume that $\sigma_n=\sigma_s$, $\delta_n=\delta_s$ and $\Gamma_n=\Gamma_s$. In all simulations, $\sigma_n=400$ MPa and $\delta_n=1$ nm. The interfacial toughness Γ_n is varied between 0.5 J/m^2 and 10 J/m^2. The bonded interface is meshed with four-node cohesive elements sharing nodes with the neighboring elements in the film and the substrate. To simulate the brittle fracture initiation and propagation at the crest of the buckled film, extended finite element method (XFEM) is employed to enrich the film elements along the centerline of the film. Maximum principal stress criterion for crack initiation is used with the film strength set to be 2 GPa. Viscous regularization option in ABAQUS is used for both the cohesive elements and the XFEM enrichment to enhance computation convergence.

Fig. 5 plots the map of buckling-driven failure modes in the parameter space of interfacial adhesion energy and initial imperfection size, for various Young's Moduli of the substrate E_s. Emerging from the simulation results are the same three failure modes as revealed from the theoretical analysis (i.e., Fig. 3) (videos showing full failure process of these three modes are available at: http://ter.ps/ModeA, http://ter.ps/ModeB, and http://ter.ps/ModeC, respectively). Simulation results show that, as the substrate becomes more compliant, Modes A and B become more dominant in the parameter space explored. That is, buckling-driven film cracking is more likely to occur.

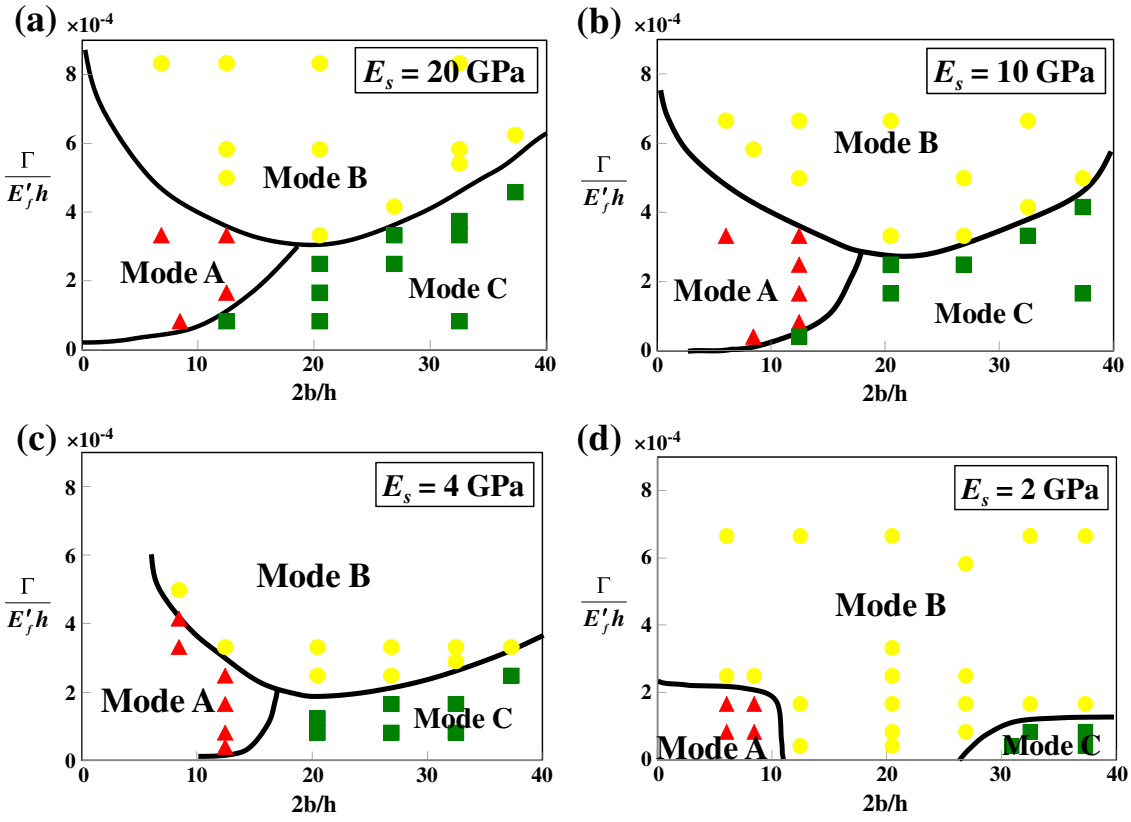

Fig. 5. (a–d). The map of buckling-driven failure modes (same as those defined in Fig. 3) in the parameter space of interfacial adhesion energy and initial interfacial defect size, for various substrate stiffness. Each mark indicates a finite element simulation case, with triangles denoting Mode A, disks denoting Mode B and squares denoting Mode C. The boundary lines between different failure modes are estimated from the simulation results.

The effect of substrate stiffness can be understood as follows. As the substrate becomes more compliant, the deformation of the film near the edges of delamination front is less constrained. In other words, the substrate can more easily deform locally to accommodate out-of-plane buckling of the film, which on one hand leads to increasing buckling amplitude, and on the other hand results in decreasing driving force for further advancement of delamination. In Fig. 3, there exists a critical interfacial adhesion energy (indicated by the horizontal boundary between Mode A and Mode C), below which no film cracking occurs (i.e., Mode C), no matter what the size of the initial delamination is. By contrast, as shown in Fig. 5, if the size of initial delamination is too small, Mode A or B dominates, which eventually leads to film cracking, no matter how weak the interfacial adhesion is. That is, to avoid buckling-driven cracking of a brittle film supported by a rather compliant substrate, a long initial interfacial delamination and a weak interfacial adhesion are desired to allow Mode C to occur. For example, in Fig. 1a, $2b/h \approx 6.4$, while in Fig. 1b, $2b/h \approx 174$. Taking $E_s = 2$ GPa, a representative stiffness for polyimide, Fig. 5d suggests buckling-driven film cracking after delamination advances (Mode A) in Fig. 1a and buckling-driven delamination without film cracking (Mode C) in Fig. 1b, assuming a weak interfacial adhesion. In this sense, the model prediction agrees well with the experimental observations.

5. Concluding remarks

In summary, through theoretical analysis and numerical modeling, we identify three buckling-driven failure modes in substrate-supported thin brittle films, two of which eventually leads to film cracking and the third involves only buckling-driven delamination without film cracking. These three failure modes are mapped out in the parameter space of interfacial adhesion energy and initial interfacial defect size. As the substrate becomes more compliant, the failure modes leading to film cracking become more dominant against the delamination-only failure mode. Interestingly emerging from the results is that, a thin brittle film strongly bonded on a substrate is indeed more prone to buckling-driven cracking, a more detrimental failure mode for transparent ITO conductors widely used in displays and flexible electronics. In this sense, the present study offers guidelines on optimal material selection and adhesion control in designing functional thin brittle films in microelectronics and flexible electronics devices.

Acknowledgment

This work is supported by NSF Collaborative Research Grant (Nos. 0928278 and 0928297). T.L. also acknowledges the support of NSF (Grant No. 0856540). Z.J. acknowledges UMD Future Faculty Program and a student travel award from the Haythornthwaite Foundation. We thank Rui Huang for helpful discussion.

References

[1] W.D. Nix, Metall. Trans. A Phys. Metall. Mater. Sci. 20 (1989) 2217.
[2] J.W. Hutchinson, Z. Suo, Adv. Appl. Mech. 29 (1992) 63.
[3] S.P. Lacour, J. Jones, S. Wagner, T. Li, Z. Suo, Proc. IEEE 93 (2005) 1459.
[4] J.A. Rogers, T. Someya, Y.G. Huang, Science 327 (2010) 1603.
[5] Y. Leterrier, Prog. Mater. Sci. 48 (2003) 1.
[6] D.R. Cairns, G.P. Crawford, Proc. IEEE 93 (2005) 1451.
[7] C. Peng, Z. Jia, D. Bianculli, T. Li, J. Lou, J. Appl. Phys. 109 (2011) 103530.
[8] N. Bowden, S. Brittain, A.G. Evans, J.W. Hutchinson, G.M. Whitesides, Nature 393 (1998) 146.
[9] Z.Y. Huang, W. Hong, Z. Suo, J. Mech. Phys. Solids 53 (2005) 2101.
[10] R. Huang, J. Mech. Phys. Solids 53 (2005) 63.
[11] D.-Y. Khang, H. Jiang, Y. Huang, J. Rogers, Science 311 (2006) 208.
[12] J.W. Hutchinson, M.D. Thouless, E.G. Liniger, Acta Metall. Mater. 40 (1992) 295.
[13] M.D. Thouless, J.W. Hutchinson, E.G. Liniger, Acta Metall. Mater. 40 (1992) 2639.
[14] H.H. Yu, M.Y. He, J.W. Hutchinson, Acta Mater. 49 (2001) 93.
[15] H.H. Yu, J.W. Hutchinson, Int. J. Fract. 113 (2002) 39.
[16] H.X. Mei, R. Huang, J.Y. Chung, C.M. Stafford, H.H. Yu, Appl. Phys. Lett. 90 (2007) 151902.
[17] M.J. Cordill, D.F. Bahr, N.R. Moody, W.W. Gerberich, Mater. Sci. Eng., A 443 (2007) 150.
[18] M.D. Thouless, J. Am. Ceram. Soc. 76 (1993) 2936.
[19] B. Cotterell, Z. Chen, Int. J. Fract. 104 (2000) 169.
[20] S. Faulhaber, C. Mercer, M.W. Moon, J.W. Hutchinson, A.G. Evans, J. Mech. Phys. Solids 54 (2006) 1004.
[21] H.J. Kim, M.W. Moon, D.I. Kim, K.R. Lee, K.H. Oh, Scr. Mater. 57 (2006) 1016.